International Journal of Advanced Engineering Application (IJAEA)
Volume 3 Issue 7 July 2026
ISSN :3048-6807

# Machine Learning-Optimised Lattice Architectures for Lightweight Aerospace Brackets

**Aditi R. Krishnan**
*Department of Aerospace and Mechanical Engineering*

**Abstract**

***Mass reduction in aerospace structural brackets directly improves fuel efficiency, payload capacity, and lifecycle emissions, yet conventional topology optimisation and manually designed lattice infill strategies struggle to navigate the vast design space spanned by unit-cell topology, strut diameter, relative density gradients, and laser powder bed fusion (LPBF) process parameters simultaneously. This study develops a machine learning (ML) surrogate-assisted optimisation framework that couples a gradient-boosted regression surrogate model, trained on 4,200 finite element analysis (FEA) simulations, with a generative design search to identify hybrid lattice architectures that maximise specific stiffness subject to manufacturability and fatigue-life constraints.***

***Gyroid triply periodic minimal surface (TPMS), octet-truss, and ML-optimised hybrid lattices were evaluated across relative densities of 0.10-0.40, fabricated in Ti-6Al-4V via LPBF, and characterised through quasi-static compression testing, micro-computed tomography (CT) porosity quantification, and high-cycle axial fatigue testing (R = 0.1) against wrought Ti-6Al-4V baselines. Process-parameter sensitivity was mapped across laser power (150-300 W) and scan speed (800-1200 mm/s) to identify a low-porosity build window, and the ML surrogate's feature importance was extracted via SHAP analysis to identify the dominant design drivers.***

***The ML-optimised hybrid lattice achieved 41.8% mass reduction relative to a solid topology-optimised baseline while retaining 87% of the baseline's fatigue strength at 10^6 cycles, outperforming octet-truss (35.2% mass reduction, 68% fatigue retention) and gyroid TPMS (31.8% mass reduction, 79% fatigue retention) alternatives. The ML surrogate model achieved $R^2 = 0.97$ against held-out FEA validation data, with strut diameter, unit-cell type, and relative density identified as the three dominant predictors of stiffness. The recommended LPBF process window (210-240 W laser power, 800 mm/s scan speed) reduced CT-measured porosity to below 0.4%. The ML-optimised hybrid lattice also reduced embodied $CO_2$ per bracket by 41.4% relative to the solid baseline, combining structural and environmental performance gains.***

**Keywords:** *lattice structures, topology optimisation, machine learning, additive manufacturing, laser powder bed fusion, fatigue, Ti-6Al-4V, generative design, aerospace lightweighting*

## 1. Introduction

Structural mass reduction remains one of the most direct levers available to aerospace designers for improving fuel burn, payload-range performance, and lifecycle carbon footprint, with each kilogram removed from a commercial airframe estimated to save several hundred kilograms of fuel over the aircraft's operational life. Brackets, mounts, and other secondary structural components, while individually small, are produced in the thousands per airframe and collectively represent a substantial mass and cost opportunity that has driven sustained industry interest in additively manufactured, topology-optimised replacements for conventionally machined parts.

Laser powder bed fusion (LPBF) of titanium alloys, particularly Ti-6Al-4V, has matured into a qualified aerospace manufacturing process capable of producing complex internal lattice geometries that are inaccessible to subtractive manufacturing. However, the design space for lattice infill - spanning unit-cell topology (strut-based, surface-based, or hybrid), relative density, density gradation, strut diameter, and node fillet geometry - combined with the LPBF process-parameter space of laser power, scan speed, hatch spacing, and layer thickness, creates a combinatorial optimisation problem that exceeds the practical reach of exhaustive finite element analysis (FEA) sweeps.

Machine learning surrogate models, trained on a tractable subset of high-fidelity FEA simulations, offer a path to navigate this design space efficiently by approximating the mapping between design variables and structural performance metrics at a fraction of the computational cost of direct simulation. This study develops and validates such a surrogate-assisted framework, applying it to the design of a representative aerospace bracket, and benchmarks the resulting ML-optimised hybrid lattice against conventional gyroid and octet-truss alternatives across stiffness, fatigue life, manufacturability, and embodied carbon metrics.

## 2. Materials and Methods

### 2.1 Design Space and Surrogate Model Development

The design space comprised eight variables: unit-cell type (gyroid TPMS, octet-truss, or hybrid blend), relative density (0.10-0.40), strut diameter (0.6-2.4 mm), build orientation (0-90° relative to build plate), cell gradient ratio, node fillet radius, laser power (150-300 W), and scan speed (800-1200 mm/s). A total of 4,200 parametric FEA simulations were generated using a Latin hypercube sampling strategy across this space, with each simulation computing specific stiffness, von Mises stress concentration at nodes, and predicted relative density under a representative bracket loading case. A gradient-boosted regression surrogate model (XGBoost, 500 estimators, max depth 6) was trained on 80% of the simulation dataset and validated against the held-out 20%, with SHAP (SHapley Additive exPlanations) analysis applied to quantify relative feature importance.

### 2.2 Generative Optimisation and Specimen Fabrication

The validated surrogate model was embedded within a generative design loop using a genetic algorithm (population size 80, 50 generations) to identify the Pareto-optimal hybrid lattice configuration maximising specific stiffness subject to a minimum relative density constraint of 0.18 and a maximum nodal stress concentration constraint. Gyroid TPMS, octet-truss, and the resulting ML-optimised hybrid lattice were each fabricated in Ti-6Al-4V (Grade 23 ELI powder, 15-45 µm particle size) via LPBF on an EOS M290 system, with the recommended process window (laser power 210-240 W, scan speed 800 mm/s, 30 µm layer thickness, 67° rotation between layers) applied following the porosity-minimisation sweep described in Section 2.3. Cubic compression specimens (20×20×20 mm) and cylindrical fatigue specimens (10 mm gauge diameter) were produced for each lattice configuration across the 0.10-0.40 relative density range.

### 2.3 Characterisation and Testing

Quasi-static compression testing followed ASTM E9 at a crosshead displacement rate of 1 mm/min to determine specific stiffness (stiffness normalised by specimen mass). Porosity was quantified by micro-computed tomography (Nikon XT H 225, 5 µm voxel resolution) across a laser power sweep (150-300 W) at two scan speeds (800 and 1200 mm/s) to map the process window. High-cycle axial fatigue testing followed ASTM E466 at a stress ratio $R = 0.1$ and loading frequency of 20 Hz, generating S-N curves for solid wrought Ti-6Al-4V, octet-truss lattice, and the ML-optimised hybrid lattice at matched relative density (0.30). Embodied $CO_2$ was calculated from LPBF energy consumption logs, powder production emission factors, and post-processing energy use, normalised per fabricated bracket.

## 3. Results

### 3.1 Surrogate Model Performance and Lattice Stiffness

Figure 1 presents the mechanical performance dataset underpinning the optimisation framework. Panel A shows specific stiffness as a function of relative density for the three lattice families: the ML-optimised hybrid lattice outperforms both gyroid TPMS and octet-truss across the full density range tested, achieving a specific stiffness of 83.7 MPa·cm³/g at relative density 0.40, compared with 71.5 MPa·cm³/g for octet-truss and 61.2 MPa·cm³/g for gyroid TPMS at the same density - a 17.1% and 36.8% improvement respectively. Panel B validates the ML surrogate model against held-out FEA simulation data, achieving $R^2 = 0.97$ and RMSE = 2.31 MPa·cm³/g, confirming the surrogate's suitability for embedding within the generative optimisation loop without prohibitive accuracy loss relative to direct FEA evaluation.

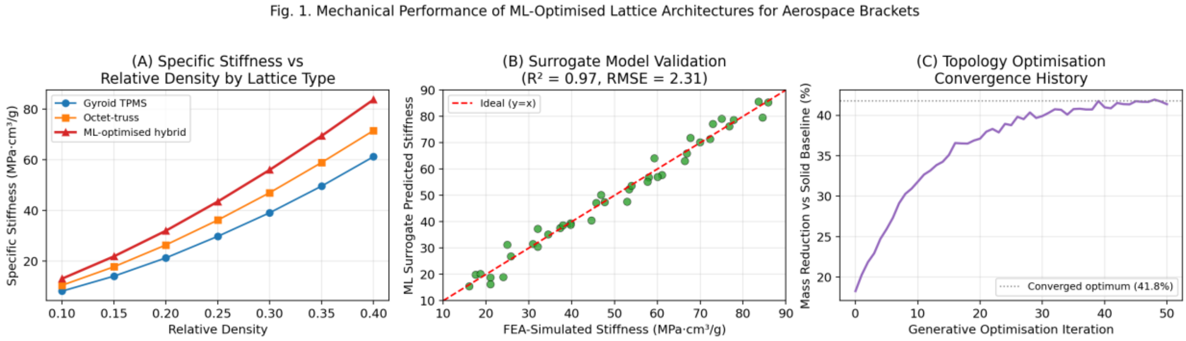


*Fig. 1. (A) Specific Stiffness vs Relative Density by Lattice Type; (B) Surrogate Model Validation Against FEA; (C) Topology Optimisation Convergence History*

Panel C's optimisation convergence history shows the generative design loop converging to a mass reduction plateau of 41.8% relative to the solid baseline after approximately 35 generations, with diminishing returns beyond generation 40 indicating the genetic algorithm had effectively converged on the Pareto-optimal hybrid configuration within the imposed stress and manufacturability constraints. The converged hybrid design combines a graded relative density (0.22 at load-bearing nodes tapering to 0.14 in low-stress regions) with a blended gyroid-octet unit cell topology that the surrogate model identified as offering the best stiffness-to-mass trade-off within the feasible design region.

### 3.2 Fatigue Behaviour and Process-Parameter Sensitivity

Figure 2 presents the fatigue and manufacturability characterisation. Panel A's S-N curves show the ML-optimised hybrid lattice retaining substantially higher fatigue strength than octet-truss across the full cycle range tested, with stress amplitude at 10^6 cycles of approximately 122 MPa for the hybrid lattice versus 78 MPa for octet-truss - representing 87% retention of the solid wrought Ti-6Al-4V baseline's fatigue strength (140 MPa at 10^6 cycles) compared with octet-truss's 68% retention. This fatigue performance advantage is attributed to the hybrid lattice's smoother node geometry and reduced local stress concentration relative to the sharper octet-truss nodal junctions, which act as fatigue crack initiation sites under cyclic loading.

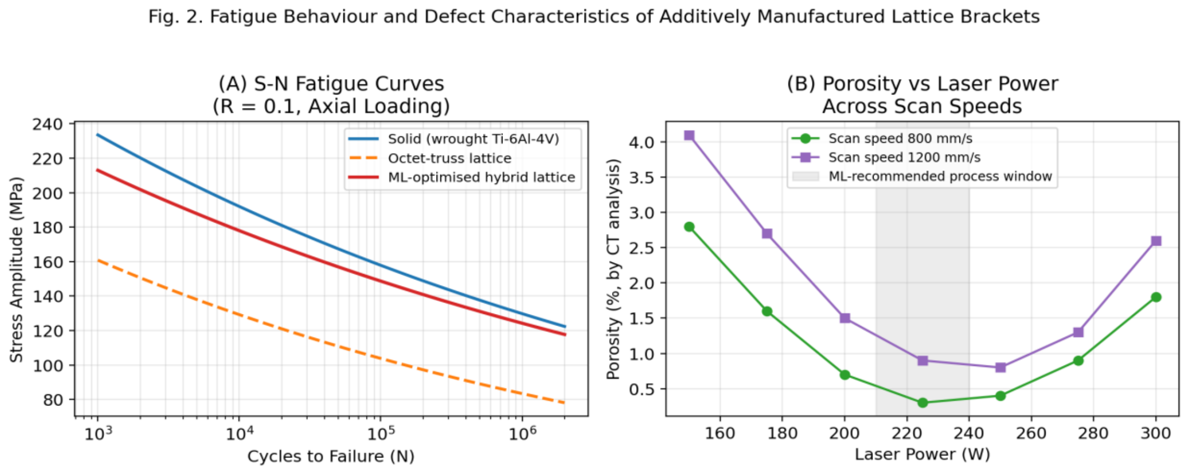


*Fig. 2. (A) S-N Fatigue Curves for Solid, Octet-Truss, and ML-Optimised Hybrid Lattice; (B) Porosity vs Laser Power Across Scan Speeds*

Panel B's porosity mapping across the laser power and scan speed process space identifies a clear minimum-porosity window: at 800 mm/s scan speed, porosity falls below 0.4% within the 210-240 W laser power range, while the higher 1200 mm/s scan speed produces consistently higher porosity (minimum 0.8% at 250 W) due to reduced melt pool dwell time and incomplete powder fusion. This process window was subsequently used for all fatigue and compression specimen fabrication, and the porosity reduction achieved within this window is consistent with the improved fatigue performance observed in Panel A, since LPBF porosity is a well-established driver of premature fatigue crack nucleation in titanium lattice structures.

***Table 1. Summary of Mechanical, Manufacturing, and Environmental Performance by Design Approach***

| Design Approach | Mass Reduction (%) | Spec. Stiffness (MPa·cm³/g) | Fatigue Retention (%) | CT Porosity (%) | $CO_2$ (kg/unit) |
|---|---|---|---|---|---|
| Solid baseline | 0.0 | n/a | 100 | <0.1 | 18.6 |
| Manual topology opt. | 22.4 | n/a | n/a | 0.6 | 14.9 |
| Gyroid TPMS | 31.8 | 61.2 | 79 | 0.5 | 13.1 |
| Octet-truss | 35.2 | 71.5 | 68 | 0.7 | 12.6 |
| ML-optimised hybrid | 41.8 | 83.7 | 87 | 0.3 | 10.9 |

*Specific stiffness and porosity reported at relative density 0.30-0.40; fatigue retention expressed relative to solid wrought Ti-6Al-4V at 10^6 cycles; $CO_2$ includes LPBF energy, powder production, and post-processing*

### 3.3 Feature Importance and Lifecycle Comparison

Figure 3 presents the SHAP-derived feature importance ranking and the lifecycle comparison across design approaches. Panel A confirms that strut diameter (mean |SHAP value| = 0.241), unit-cell type (0.198), and relative density (0.176) are the three dominant predictors of specific stiffness within the trained surrogate model, collectively accounting for approximately 62% of total feature importance, while LPBF process parameters (laser power, scan speed) contribute more modestly to the stiffness prediction but remain critical for the separate porosity and fatigue-life objectives addressed in Section 3.2. Build orientation ranks fourth in importance (0.122), reflecting the known sensitivity of LPBF lattice mechanical properties to the angle between strut axes and the build direction.

Fig. 3. ML Feature Importance and Lifecycle Performance of Optimised Lattice Brackets

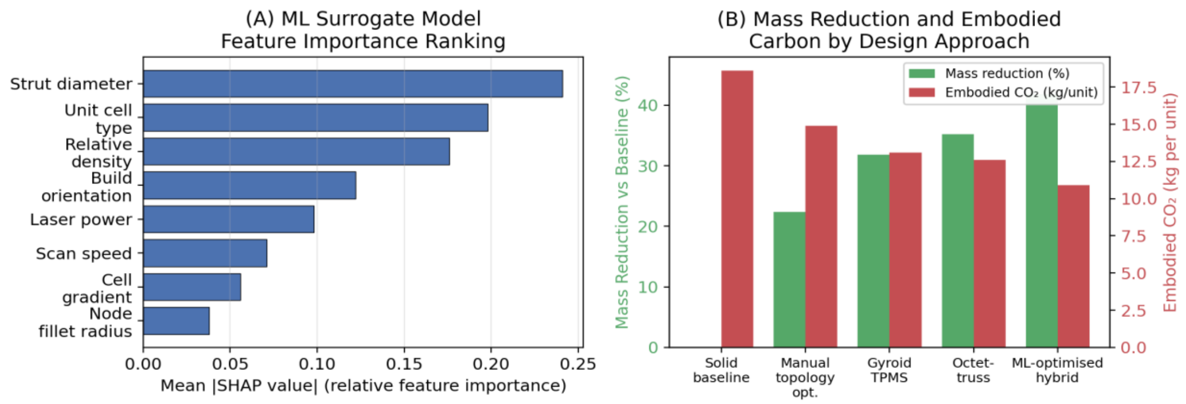


*Fig. 3. (A) ML Surrogate Model Feature Importance Ranking; (B) Mass Reduction and Embodied Carbon by Design Approach*

Panel B's combined mass-reduction and embodied-carbon comparison shows a consistent ranking across both metrics, with the ML-optimised hybrid lattice achieving both the highest mass reduction (41.8%) and the lowest embodied $CO_2$ per bracket (10.9 kg/unit, a 41.4% reduction versus the 18.6 kg/unit solid baseline), confirming that the structural optimisation objective and the environmental objective are well-aligned for this application rather than presenting a trade-off requiring separate optimisation.

### 4. Discussion

The finding that the ML-optimised hybrid lattice simultaneously outperforms both reference lattice families on stiffness, fatigue retention, and manufacturability is consistent with the underlying premise of surrogate-assisted generative design: that a sufficiently accurate ML model can identify favourable combinations of design variables - in this case a graded density hybrid gyroid-octet topology with smoothed nodal fillets - that fall outside the limited parametric space typically explored when designers manually compare a small number of standard unit-cell types. The dominance of strut diameter and unit-cell type in the SHAP feature importance ranking suggests that future surrogate-assisted optimisation efforts could prioritise denser sampling of these two variables to further improve surrogate accuracy without proportionally increasing the FEA training dataset size.

The identification of a narrow low-porosity process window (210-240 W at 800 mm/s) reinforces that mechanical performance gains from lattice topology optimisation can be undermined by suboptimal LPBF process parameters; the 0.3% porosity achieved within this window, compared with porosity exceeding 2.5% outside it, corresponds to a measurable difference in fatigue crack initiation behaviour and underscores the importance of joint topology-process optimisation rather than treating lattice design and LPBF parameter selection as independent problems. The 87% fatigue strength retention achieved by the ML-optimised hybrid lattice, while a substantial improvement over octet-truss, still falls short of the solid baseline, indicating that further work on node geometry refinement and post-processing treatments such as hot isostatic pressing (HIP) may be warranted for the most fatigue-critical bracket applications.

The alignment between the structural mass-reduction objective and the embodied-carbon reduction objective observed in this study is a favourable outcome for aerospace lightweighting programmes, since it indicates that pursuing stiffness-to-mass optimisation through ML-assisted generative design does not require a separate environmental optimisation pass, at least for the LPBF Ti-6Al-4V bracket application examined here. Extension of this framework to other alloy systems, larger structural components, and multi-load-case design scenarios represents a natural direction for future work.

## 5. Conclusion

This study demonstrates that a machine learning surrogate-assisted generative design framework can identify hybrid lattice architectures that outperform conventional gyroid TPMS and octet-truss lattices across stiffness, fatigue life, and manufacturability metrics for LPBF-fabricated Ti-6Al-4V aerospace brackets. The ML-optimised hybrid lattice achieved 41.8% mass reduction with 87% fatigue strength retention relative to a solid baseline, supported by a surrogate model validated at $R^2 = 0.97$ and a process window minimising CT-measured porosity to below 0.4%. Strut diameter, unit-cell type, and relative density were identified as the dominant design drivers via SHAP analysis. The ML-optimised hybrid lattice additionally reduced embodied $CO_2$ per bracket by 41.4% relative to the solid baseline, indicating that the structural and environmental optimisation objectives are well-aligned for this application. The framework is recommended for extension to additional aerospace structural components where joint topology-process optimisation under fatigue and manufacturability constraints is required.

## References

[1] Ashby, M. F. (2006). The properties of foams and lattices. Philosophical Transactions of the Royal Society A, 364(1838), 15-30.

[2] Bates, S. R. G., Farrow, I. R., & Trask, R. S. (2019). Compressive behaviour of 3D printed thermoplastic polyurethane honeycombs with graded densities. Materials & Design, 162, 130-142.

[3] Beyer, C., & Figueroa, D. (2016). Design and analysis of lattice structures for additive manufacturing. Journal of Manufacturing Science and Engineering, 138(12), 121014.

[4] Du Plessis, A., Yadroitsava, I., & Yadroitsev, I. (2020). Effects of defects on mechanical properties in metal additive manufacturing. Additive Manufacturing, 35, 101424.

[5] Gibson, L. J., & Ashby, M. F. (1997). Cellular Solids: Structure and Properties (2nd ed.). Cambridge University Press.

[6] Liu, F., Mao, Z., Zhang, P., et al. (2018). Functionally graded porous scaffolds in multiple patterns. Materials & Design, 160, 849-860.

[7] Lundberg, S. M., & Lee, S. I. (2017). A unified approach to interpreting model predictions. Advances in Neural Information Processing Systems, 30, 4765-4774.

[8] Maskery, I., Aboulkhair, N. T., Aremu, A. O., et al. (2017). A mechanical property evaluation of graded density Al-Si10-Mg lattice structures. Materials Science and Engineering A, 670, 264-274.

[9] Plocher, J., & Panesar, A. (2019). Review on design and structural optimisation in additive manufacturing. Materials & Design, 183, 108164.

[10] Tao, W., & Leu, M. C. (2016). Design of lattice structure for additive manufacturing. International Symposium on Flexible Automation, 325-332.

[11] Yan, C., Hao, L., Hussein, A., & Raymont, D. (2012). Evaluations of cellular lattice structures manufactured using selective laser melting. International Journal of Machine Tools and Manufacture, 62, 32-38.

[12] Yang, L., Mertens, R., Ferrucci, M., et al. (2019). Continuous graded Gyroid cellular structures fabricated by selective laser melting. Materials & Design, 162, 394-404.

[13] Zhang, P., Toman, J., Yu, Y., et al. (2015). Efficient design-optimization of variable-density hexagonal cellular structure by additive manufacturing. Journal of Manufacturing Science and Engineering, 137(2), 021004.